Comparison Study of a Second-Generation and of a Third-Generation Wave Prediction Model in the Context of the SEMAPHORE Experiment

BÉATRICE FRADON

Météo-France, Toulouse, France

DANIÈLE HAUSER

CETP/CNRS, Velizy, France

JEAN-MICHEL LEFÈVRE

Météo-France, Toulouse, France

(Manuscript received 10 August 1998, in final form 22 February 1999)

ABSTRACT

Numerical wave prediction models presently used in the meteorological institutes are still of two types: the so-called second-generation and third-generation models. In this paper, the authors present a comparison of the performance of a second-generation model—the VAG model from Météo-France—and of the third-generation WAM model. These two models have been run with similar characteristics (same wind input, same resolution). Simple tests show the differences between the behaviors of VAG and WAM in typical situations (constant wind, rotating wind). Hindcasts have been performed in the general context of the SEMAPHORE experiment. A one-month hindcast over the North Atlantic domain has been run by driving both models with the same wind fields. A comparison between the model output and the available observations, including significant wave height from satellite measurements, is presented. The results show that VAG and WAM results are in a general good agreement with the observations, but also that WAM results are a little better than VAG when the satellite data are taken as a reference. A modification of VAG is then proposed, which allows the performances of VAG to be closer to those of WAM. This study shows that (i) the second-generation VAG model is nearly as good in predicting wave heights as the third-generation model WAM in spite of its poor representation of the nonlinear interactions and (ii) VAG has been improved when introducing the growth and dissipation terms of WAM instead of parameterizations taken from Golding.

1. Introduction

The usefulness of wave prediction models is proven. For several decades, security and economic applications have required the knowledge of the mean sea state or the prediction of wave spectra. More recently, some scientific applications have been developed, due to the interest given to the ocean–atmosphere interactions and to the development of satellite techniques.

The evolution of the sea state has been studied since the 1950s. The first theories giving a precise description of the development of the wave energy spectra were those of Phillips (1957) and Miles (1957). Both theories gave an expression of the energy source term due to the wind. This term, as given by Phillips, results in a linear growth of the wave energy, whereas Miles' expression results in an exponential growth. Some other and more sophisticated expressions were proposed later for the wind input term (Janssen 1989) but Phillips and Miles' expressions remain quite widely used. Some theories also gave expressions for the dissipation source term—for example, Hasselmann (1974), Phillips (1985), Donelan and Pierson (1987), and Longuet-Higgins (1969). Finally, the nonlinear interactions were mainly studied by Hasselmann (1962).

Concurrent to the development of these theories, some measurements were collected and used to describe the phenomena involved in the evolution of the wave spectrum and the typical shapes of the spectra. The observations made by Snyder et al. (1981) allowed a better knowledge of the wind input term. The Joint North Sea Wave Project (JONSWAP) experiment (Hasselmann et al. 1973) also gave a better understanding of the source terms and the general shape of the wave spectra. Based on these experiments and on the theories of the wave

Corresponding author address: Béatrice Fradon, SCEM/PREVI/CDMA, Météo-France, 42 Avenue Coriolis, Toulouse, Cedex F-31057, France.
E-mail: beatrice.fradon@meteo.fr

evolution, some reference spectra were defined, as the Phillips spectrum (Phillips 1977), the Pierson–Moskowitz spectrum (Pierson and Moskowitz 1964), the JONSWAP spectrum (Hasselmann et al. 1973), and the Donelan spectrum (Donelan et al. 1985).

The development of the numerical wave prediction models followed the improvements in the knowledge of the processes involved in the wave evolution. The first-generation models were very simple and did not take into account the nonlinear interactions or did so very simply. The second-generation models did take them into account but only through parameterizations. In the third-generation models, an explicit source term for the nonlinear interactions is included, using the method developed by Hasselmann et al. (1985). So, second-generation models should be more accurate than first-generation ones, and third-generation models should be the most accurate. Although third-generation wave models have a better representation of the physics, it has not been demonstrated that second-generation wave models are inadequate for operational applications, particularly since computational efficiency is important here (Holt 1994).

The implementation of a new model, and in particular of a third generation, requires more personnel and computation resources. Moreover, the increasing availability of satellite data motivates the development of techniques of data assimilation in wave models. The use of the most efficient ones requires a large number of model integrations. The question then arises in the interest of implementing an assimilation scheme in a third-generation wave model for operational forecast, rather than in a second-generation model.

Consequently, the purpose of this study is to attempt to better answer this question, taking advantage of a large dataset from an experiment. Two models were used: the second-generation VAG used at Météo-France (Guillaume 1990) and the third-generation Wave Model (WAM) used at the European Centre for Medium-Range Weather Forecasts (ECMWF) (WAMDI Group 1988). The purpose was to compare the models outputs with each other and with observations. The aim was also to propose possible improvements for VAG. The period chosen for this study corresponds to the one of the SEMAPHORE experiments, which took place in the North Atlantic (between Madeira and the Azores) in October–November 1993 (Eymard et al. 1996). From this experiment both wind and wave measurements were obtained and used in the present study. Moreover, wind and wave data from satellite measurements (TOPEX/Poseidon, *ERS-1*) have been used in this study in order to extend the possibility of comparisons between model outputs and observations.

Section 2 presents VAG and WAM and some basic tests. Section 3 gives a brief description of the SEMAPHORE experiment and of the wind fields and observations used in this study. Section 4 presents the results of hindcasts made with VAG and WAM during the period of the SEMAPHORE experiment. Sections 5 and 6 give the modification made to improve VAG and the results of the hindcasts made with this new version of VAG. Finally, section 7 gives a summary of this study.

2. General characteristics of the VAG and WAM models

Both models used in the present study were developed to be used on operational basis. VAG is a second-generation wave prediction model developed in the 1980s at Météo-France (Guillaume 1990). WAM is a third-generation wave prediction model developed in 1988 at ECMWF (WAMDI Group 1988).

Both models are based on the solution of the equation for the conservation of action (Phillips 1977). The following sections (2a–2b) give more details about these models, and Table 1 presents the configuration of the models used in the present study.

a. The VAG model

The operational version of VAG is run on a polar stereographic grid on the North Atlantic Ocean, assuming deep water at each grid point.

The VAG version used in the study presented here uses a spherical 0.5° grid. The second-order advection scheme implemented in the operational version was replaced here by a first-order scheme, which tends to smooth the garden sprinkler effect. This version will soon become operational. It will simply be referred to as VAG in the following.

Under the deep water assumption and without current, the equation for the conservation of wave action can be simplified to obtain the following equation for the evolution of the wave spectrum $F(f, \theta)$:

$$\frac{\partial F(f, \theta)}{\partial t} + \mathbf{c}_g \cdot \nabla F(f, \theta) + \frac{\partial}{\partial \theta}[(\mathbf{c}_g \cdot \nabla \theta) F(f, \theta)] = S(f, \theta), \quad (1)$$

where f and θ the wave frequency and propagation direction, respectively; $\mathbf{c}_g$ their group velocity; and S the source/sink term.

The physical part of the model is identical to the one used in the operational version of VAG: the source/sink term $S(f, \theta)$ consists of a linear growth term, S_{lin}, representing the Phillips' growth process (Phillips 1957); an exponential growth term, S_{exp}, representing the Miles' growth (Miles 1957); and a dissipation term, S_{dis}, representing dissipation due to wave breaking as given by Golding (1983). The expressions for these source or sink terms are detailed in the appendix.

The effects of the nonlinear interactions are taken into account in an indirect way that consists of two steps. In the first step, the region of the wave spectrum that corresponds to the wind–sea is delimited and the total

TABLE 1. Configuration for VAG and WAM in the present study.

	Configuration of VAG in the present study	Configuration of WAM in the present study	Modified version of VAG in the present study
Water depth assumption	Deep water	Deep water	Deep water
Spatial discretization Spatial domain	Spherical grid, 0.5° × 0.5° (10°–70°N), (80°W–10°E)	Spherical grid 0.5° × 0.5° (10°–70°N), (80°W–10°E)	Spherical grid, 0.5° × 0.5° (10°–70°N), (80°W–10°E)
Numerical scheme	Advection: first-order upstream Source term: explicit scheme	Advection: first-order upstream Source term: implicit scheme	Advection: first-order upstream Source term: explicit scheme
Time step	15 min	15 min	15 min
Number of frequency bands/ frequency range	22, geometric progression 0.040–0.296 Hz	25, geometric progression 0.0418–0.412 Hz	22, geometric progression 0.040–0.296 Hz
Number of direction bands	18	18	18
Growth term	Linear (Golding 1983) + exponential (Snyder et al. 1981)	Exponential (Janssen 1991) but without the wind–wave coupling	Exponential (Janssen 1991) but without the wind–wave coupling
Dissipation term	Golding 1983	Hasselmann (1974) modified	Hasselmann (1974) modified
Nonlinear interaction term	Not explicit	Hasselmann et al. 1985	Not explicit

energy of this domain is limited if necessary by the total energy of the Pierson–Moskowitz spectrum (Pierson and Moskowitz 1964) corresponding to the fully developed spectrum associated with the specified wind speed. This is the ''limitation of the wind–sea energy,'' which aims to avoid imbalances between growth and decay. In the second step of calculation, the wind–sea part of the spectrum is reshaped into a JONSWAP spectrum (Hasselmann et al. 1973) with a $\cos^2$ distribution on each side of the wind direction. This is the ''redistribution of the wind–sea energy.'' The configuration (resolution, domain, etc.) as used in the present study is given in Table 1.

b. The WAM model

The WAM source codes offers a range of possibilities (deep or shallow water, spherical or stereographic grid, etc.) but in this study we chose to make VAG and WAM be as close as possible (see Table 1). So WAM was used in a deep water mode on the same spherical grid as VAG and with the same first-order propagation scheme. However, the physical part of the WAM model differs quite appreciably from the VAG part. There is no linear growth term in WAM (the spectrum is initialized with a low-energy JONSWAP spectrum) and WAM exponential growth and dissipation terms differ from those of VAG (see the appendix for the detailed expressions used in WAM). More importantly, the main difference is that WAM includes an explicit source term for the nonlinear interactions. For the present study, WAM has been run in two versions. In the first one, the wind–wave coupling term proposed by Janssen (1991) has been kept as in the original code of WAM cycle 4. In the second case, the wind–wave coupling term has been removed (see the appendix), keeping all coefficients similar to the first version. We mainly focus on the results obtained with this second version because its configuration is closer to that of VAG. Results obtained with the complete cycle 4 version are mentioned when necessary.

c. Growth curves

A first step in this study was the comparison of the growth and decay curves obtained with VAG and WAM. These curves were obtained by running a ''one-point'' version (without advection) of each model forced by a wind constant during 48 h (two wind speed cases were studied: 18.25 and 6.75 m s^{-1}). After 48 h, the wind speed is abruptly changed to 0.25 m s^{-1} and kept to this constant value for the next hours of the simulation. The configuration of this simulation is close (although not exactly identical) to the one discussed by Günther et al. (1992) and Komen et al. (1994). The wind speed value could not be chosen exactly identical because VAG uses precalculated terms based on a discretization of wind speeds every 0.5 m s^{-1}).

The time series of the significant wave height (SWH) is plotted in Fig. 1 for VAG and Fig. 2 for WAM (upper plots). Figures 1 and 2 also show in the bottom plots the temporal evolution of the different terms of the energy budget (integrated over each time step of 15 min): linear and exponential growth, dissipation, energy limitation, and nonlinear interactions. In the case of VAG, this latter term is zero because the reshaping of the wind–sea part of the spectrum is energy conservative. The ''limitation term'' corresponds to the energy that is removed at each time step from the energy budget after growth and dissipation has taken place. For VAG, this term corresponds to the difference between the energy of the wind–sea part found after growth and dissipation and the energy of a Pierson–Moskowitz spectrum. This limitation is introduced into the physical

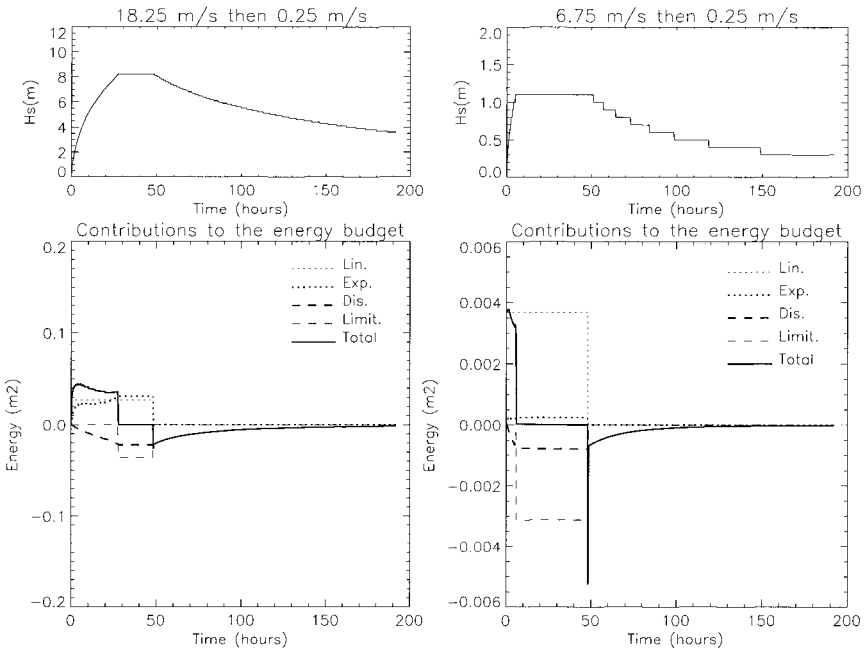

FIG. 1. Growth and decay curves obtained with VAG for wind speeds of 18.25 (left-panel) and 6.75 m s^{-1} (right panel) during the first 48 h and 0.25 m s^{-1} after 48 h. For each wind speed, the top panel shows the evolution of the SWH and the bottom panel the evolution of the different terms that contribute to the energy budget (integrated over each time step of 15 min). Legend: Sin, wind input (Lin, linear growth; Exp, exponential growth); Dis, dissipation; Snl, nonlinear interactions; Limit, limitation; Total, sum of the four terms.

scheme of VAG to avoid an infinite increase of the energy of the wind–sea part when the wind continues to blow. In WAM, a limitation is also applied to ensure numerical stability (WAMDI Group 1988; Burgers 1990), but it is applied for each frequency component, without using any criterion relative to the Pierson–Moskowitz spectrum: at each time step, the net growth rate is limited by a coefficient proportional to the inverse of the fifth power of the frequency.

As clearly shown when comparing Figs. 1 and 2, the wave growth is significantly faster in VAG than in WAM. For the 18.25 m s^{-1} wind case (left panels of Figs. 1 and 2), the significant wave height reaches its maximum after 25 h, whereas about 50 h are necessary in WAM to reach this maximum. This is even more obvious on the 6.75 m s^{-1} wind case (right panels of Figs. 1 and 2). Correlatively, the peak frequency decreases faster with time in the case of VAG with respect to WAM (not shown). These differences between VAG and WAM are similar when the wind–wave coupling is kept in WAM (not shown). WAM gives slightly better agreement with the WMO (1989) curves than VAG; for example, the maximum wave height should be observed after 36 h in the case of the 18.25 m s^{-1} wind speed, but it is observed after 25 h in VAG and the VAG peak frequency decreases too quickly. The peak frequencies in the models after the wave growth has completed are coherent with those given in WMO (1989). Figures 1 and 2 also show that when the wind stops blowing (after 48 h), the decay of the waves is also faster for VAG than for WAM.

These large differences between VAG and WAM are associated with even larger differences in the energy balance. The exponential growth and dissipation terms are about five times higher in WAM than in VAG. In the VAG model, these small terms are compensated by a very large linear growth term and a large limitation term. Experience showed (Kahma and Donelan 1988) that the linear growth term is usually negligible compared to the exponential growth one, so the high linear growth term in VAG is not very satisfactory.

The limitation term plotted in Fig. 1 for VAG shows that it reaches large values compared to the other terms of the energy balance equation. Although this limitation term is necessary as explained earlier, it is not very satisfactory to find it of the same order of magnitude as the other terms of the energy budget. This shortcoming is not found in the WAM results (Fig. 2). Note also that the limitation term of VAG (Fig. 1) presents a negative peak when the wind stops blowing. This shows a second weakness of the VAG model, which will be discussed in section 2d.

d. Effect of time-interpolated input winds

The study of the growth and decay curves for VAG and WAM evidences the importance of the limitation of the wind–sea energy in VAG. Particularly, a negative

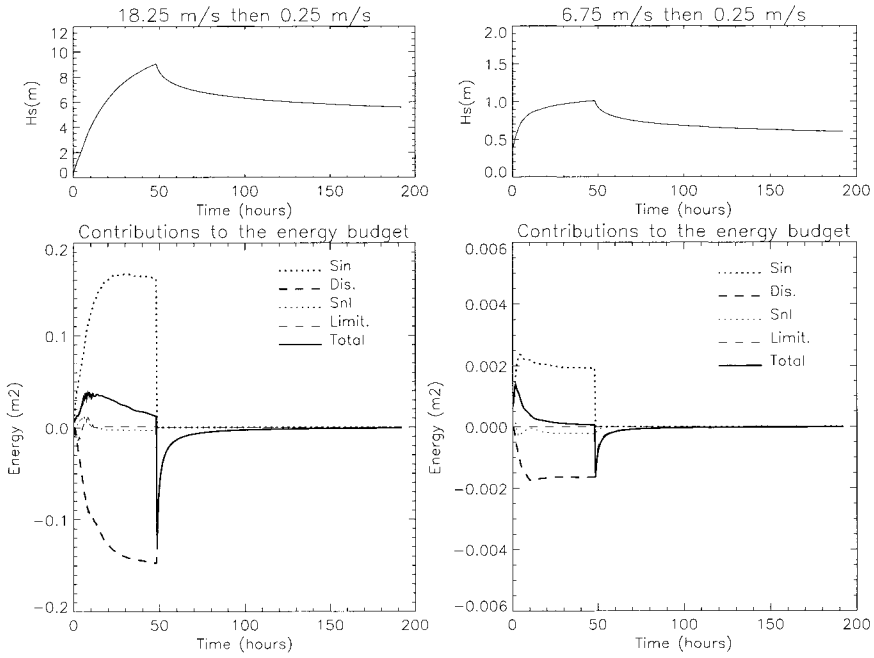

FIG. 2. As in Fig. 1 but for WAM.

peak in the limitation term of the energy budget is observed when the wind speed becomes nearly zero. In order to know whether this is due to the fact that the wind drop is instantaneous, we studied the outputs of VAG and WAM in the case of a progressive wind drop. The growth and decay of the waves were studied as in section 2c, but the wind speed was imposed to a new value every 15 min with a linear increase from 0.25 to 18.25 m s^{-1} (6.75 m s^{-1}, respectively) during 12 h, with a constant value during the next 36 h and with a linear decrease down to 0.25 m s^{-1} after a total of 48 h. Figures 3 and 4 present the temporal evolution of the SWHs and of the different terms of the energy budget in VAG and WAM corresponding to these tests.

The comparison of Figs. 2 and 4 shows that WAM is not very sensitive to a modification of the frequency of the wind forcing: using interpolated winds instead of abrupt changes in the wind speed has little impact. VAG, however, is very sensitive to such a modification (see Figs. 1 and 3), particularly for the decay of the waves, which is much quicker in the case of interpolated winds. This can be explained as follows: interpolating the winds results in a series of successive slight drops of the wind speed instead of one larger drop. Each of these slight drops results in a decrease of the energy of the Pierson–Moskowitz spectrum corresponding to the imposed wind speed. Because the energy in the wind–sea part of the spectrum is still high, the consequence is an important limitation of the wind–sea energy for each wind drop. By contrast, a single significant drop of the wind speed results in a large decrease of the energy of the Pierson–Moskowitz spectrum as well as in an important restriction of the wind–sea part of the spectrum. So the energy contained in this part of the spectrum remains generally less than the energy of the Pierson–Moskowitz spectrum and the energy limitation does not occur systematically at each time step. In WAM, the fact that there is no limitation of the energy spectrum by a given spectrum prevents from having such energy losses as in VAG. VAG is therefore much more sensitive to the frequency of the wind forcing than WAM.

e. Effect of an instantaneous rotation of the wind

In order to characterize the behavior of both models in case of a rotating wind, tests run were also performed in a way similar to those made by Young et al. (1987) and van Vledder and Holthuijsen (1993). A 11.75 m s^{-1} wind is fixed until the peak frequency of the spectrum is twice the frequency peak of the Pierson–Moskowitz spectrum, and a wind rotation of 60° is then applied. The spectra obtained 1, 3, and 6 h after the wind rotation are shown in Figs. 5 an 6 for the VAG and WAM models, respectively. The difference between the two models is obvious. In the WAM model (Fig. 6), the wave spectrum rotates slowly to align with the new wind direction within about 9 h. In the VAG model (Fig. 5), some energy migrates very quickly from the old wind direction to the new one, whereas some energy remains in the old one. The spectrum divides instantaneously into distinct wind–sea and swell parts, with a fast-growing wind–sea part. The rotation of the wind–sea part of the spectrum occurs during only one time step; so since the time step is small, this happens very quickly. Moreover, this means that the rotation of the wind–sea would be even faster if the time step of the model was reduced.

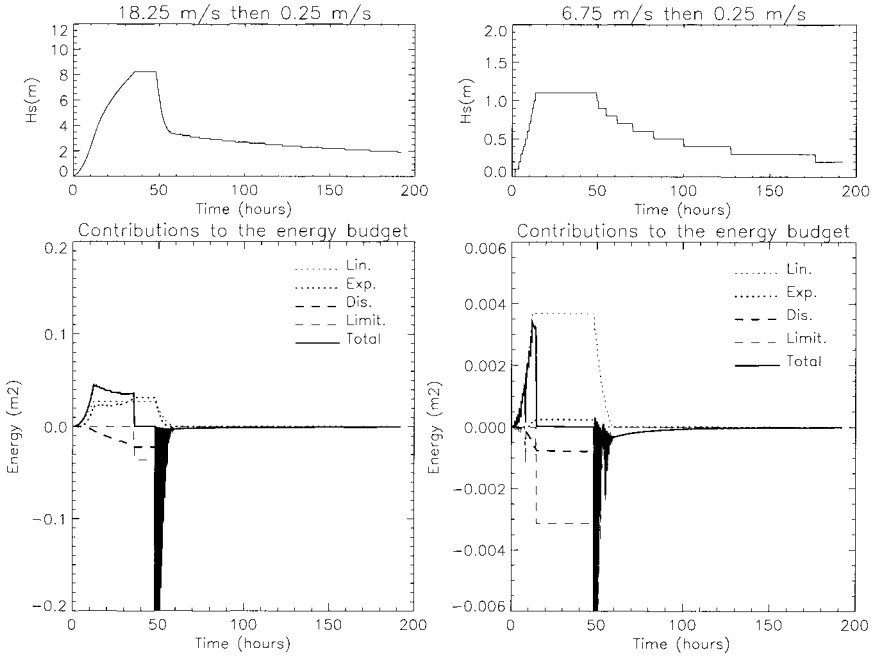

FIG. 3. As in Fig. 1, but in the case of VAG forced by a wind speed imposed to a new value every 15 min with a linear increase from 0.25 to 18.25 m s^{-1} (6.75 m s^{-1}, respectively) during 12 h, with a constant value during the next 36 h and with a linear decrease down to 0.25 m s^{-1} after a total of 48 h. The minimum values of the energy limitation are out of the scale and are -0.473 m^2 for a 18.25 m s^{-1} wind speed and -0.142 m^2 for a 6.75 m s^{-1} wind speed.

This quick creation of a new wind–sea is in disagreement with what is expected from the exact model, EXACT-NL, as used by Hasselmann and Hasselmann (1984) to represent the nonlinear interactions without simplifying assumptions. This difference between VAG and WAM is due to the treatment of the nonlinear interactions: in VAG the splitting of the total spectrum into a wind–sea part aligned with the wind direction and

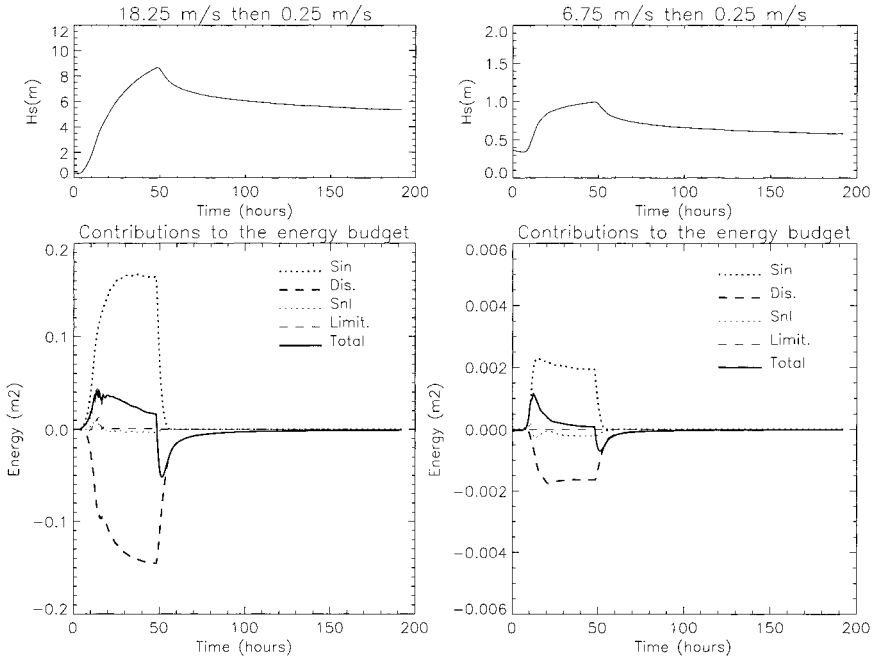

FIG. 4. As in Fig. 3 but for WAM.

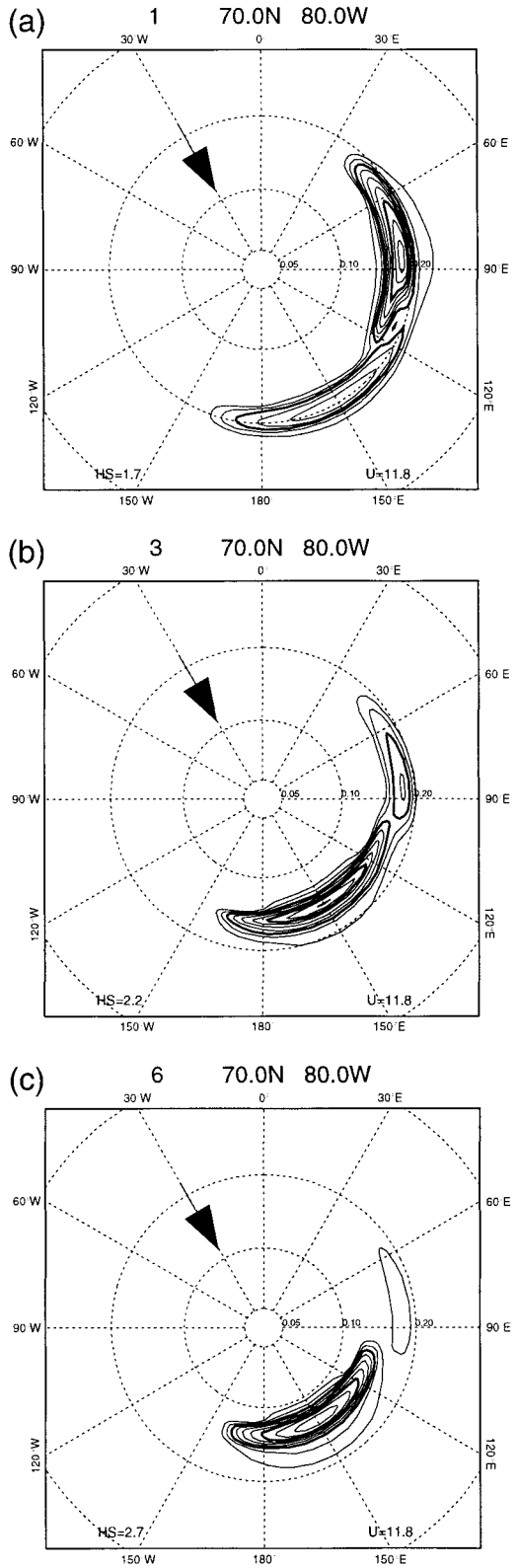

FIG. 5. Directional spectra obtained with VAG in the case of an instantaneous wind veering of 60° for a) 1 h, b) 3 h, and c) 6 h after the wind veers. The wind is blowing from the west before veering. The spectra are normalized and the isolines are plotted from 0.1 to 0.9 every 0.1. The distance to the center of the plot is proportional to the frequency of the waves, and the direction used is the one to which they propagate. The SWH is given at the bottom of each spectrum. The black arrow indicates the wind direction after its veering.

a swell part can lead to a false partitioning of the energy between wind–sea and swell. By contrast, a progressive transfer of energy from the old to the new wind–sea is obtained with the parameterization of the nonlinear interactions of WAM.

f. Effect of a progressive rotation of the wind

The same test as in section 2e was performed but the wind rotation was chosen to be progressive (60° in 6 h with change imposed every 15 min). The results indicate (not shown) that interpolating the wind direction does not have an important impact on the WAM results: the spectrum only rotates a little more slowly when the wind rotation is progressive (12 h instead of 9 h before the peak direction is aligned with the new wind direction).

For VAG, however, the impact of interpolating the wind direction is crucial. Because the spectrum is divided into a swell part and a wind–sea part at each time step, the wind–sea energy is redistributed so that the energy peak of the wind–sea always remains aligned with the wind direction. This is quite unrealistic, particularly for small time steps and a quickly rotating wind. In the case of a slow rotation of the wind, the wind–sea rotation is progressive too, which is much more satisfactory. In this latter case, the VAG results become similar to the WAM results.

So, compared to WAM, VAG is very sensitive to the frequency of the wind forcing, not only for the total energy (interpolation of the wind speed) but for the energy distribution (interpolation of the wind direction). The tests discussed in sections 2e,f show that interpolating the wind vector may result in an improvement of the model in case of changes of wind direction only, but may degrade the results in case of changes in the wind speed.

3. Observations

a. The SEMAPHORE experiment

The SEMAPHORE experiment (Eymard et al. 1996) took place from June to November 1993 in the northeast Atlantic between the Azores and Madeira, with an intensive observation period from October to November. It was designed to study the mesoscale ocean circulation and air–sea interactions. Numerous measurements were performed using drifting and moored buoys, ships, an instrumented mast on board a ship, an airborne radar, and other airborne sensors. These in situ measurements were completed by observations from the TOPEX/Po-

←

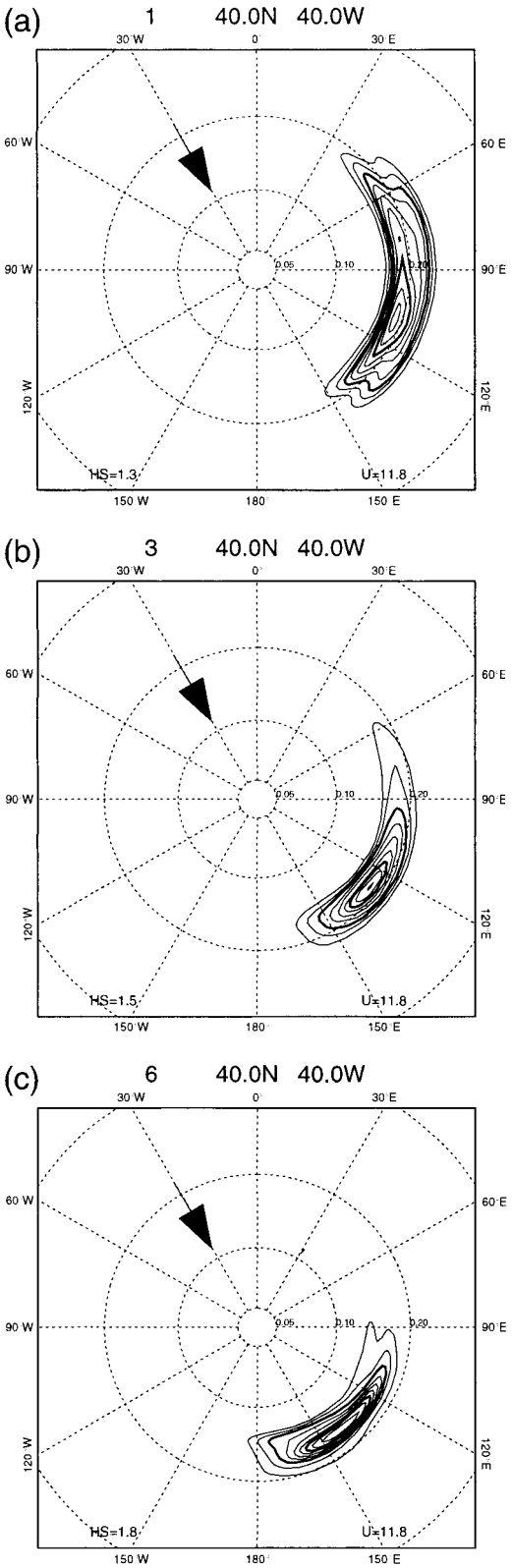

FIG. 6. As in Fig. 5 but for WAM.

seidon and *ERS-1* satellites. Ocean and wave models were also used.

b. Observations used

Only a small part of the in situ measurements are relevant for this study. We only used wind and wave data, excluding oceanographic measurements. They consisted of (Eymard et al. 1996)

- wind measurements provided by the R/V *Le Suroît* and the MARISONDE drifting buoys,
- frequency spectra of the waves from the SPEAR buoy (Datawell system), and
- directional spectra of the long waves (from 50 to 400 m) from the airborne RESSAC radar (Hauser et al. 1992; Hauser and Caudal 1996).

Moreover, some satellite measurements were used. The observations performed by the satellites are very useful because they are numerous and well distributed over the entire North Atlantic, whereas the in situ measurements were all located near the Azores. The satellite measurements used consisted of

- wind measurements provided by the *ERS-1* scatterometer and
- SWH measurements provided by the altimeters of the TOPEX/Poseidon and *ERS-1* satellites. The *ERS-1* data were the Ocean Products Records (OPRs), with the correction proposed by Tournadre et al. (1994).

The satellite altimeter data have been collocated with the VAG and WAM grid points. Every satellite data was associated with the nearest model point in time ($\pm$90 min) and in space ($\pm$0.25° in longitude and latitude). Two datasets of 15 632 values for TOPEX/Poseidon and 12 398 values for *ERS-1* were obtained using this method. The shipborne, Marisonde buoys and *ERS-1* wind observations have been used in a reanalysis process to build wind fields (see section 3c).

The significant wave heights provided by the *ERS-1* and TOPEX/Poseidon satellites have been used for comparisons with VAG and WAM outputs in order to assess the models hindcasts. Previous studies based on comparisons between satellite and buoy data show that the accuracy of satellite-derived significant wave height is about 10%. So we consider here altimeter wave heights as a reference and will compare the VAG and WAM results with this dataset.

c. The wind fields

Two types of wind fields have been used in this study to drive the wave models. The first type of wind fields, hereafter referred to as ''reanalyzed ARPEGE winds'' is based upon the use of the atmospheric model Action de Recherche Petite Echelle Grande Echelle (ARPEGE) of Météo-France (Courtier et al. 1991). The wind fields were obtained from the first guess (6-h forecast from the analysis), which was updated with the wind data

TABLE 2. Statistics of collocated datasets of reanalyzed ARPEGE wind speeds and ECMWF wind speeds with satellite measurements. Mean differences and standard deviations are in meters per second. The collocated datasets contain 15 632 collocated points for TOPEX/Poseidon and 12 398 points for *ERS-1*. The mean wind speed and standard deviation are, respectively, 7.25 and 2.68 m s^{-1} for TOPEX/Poseidon, 7.40 and 3.58 m s^{-1} for *ERS-1*, 7.13 and 3.54 m s^{-1} for the reanalyzed ARPEGE winds collocated with TOPEX/Poseidon, 7.47 and 3.58 m s^{-1} for the ECMWF winds collocated with TOPEX/Poseidon, 7.37 and 3.71 m s^{-1} for the reanalyzed ARPEGE winds collocated with *ERS-1*, and 7.67 and 3.70 m s^{-1} for ECMWF winds collocated with *ERS-1*.

	TOPEX/Poseidon			*ERS-1*		
	Mean difference	Std dev	Correlation	Mean difference	Std dev	Correlation
Reanalyzed ARPEGE winds	−0.12	2.19	0.787	−0.03	2.23	0.814
ECMWF winds	0.22	2.06	0.821	0.27	2.02	0.846

provided by the ships and buoys deployed during the campaign and by the *ERS-1* scatterometer (Le Meur et al. 1994). All the available wind data from ships and buoys were used in this reanalysis, even if they would have arrived too late for a real-time analysis. Reanalyzed ARPEGE winds are available for the entire North Atlantic with a 0.5° resolution every 6 h. No wind estimates from satellite altimeter measurements were used for these reanalyses.

The second type of wind fields—hereafter referred to as ECMWF winds—corresponds to the output of the operational atmospheric model used at ECMWF. The wind data provided by the ships and buoys deployed during the campaign were also assimilated in the ECMWF atmospheric model but it was an operational assimilation (only data transmitted in time are taken into account in the assimilation). ECMWF winds are available with a 1° resolution and have been then linearly interpolated on the 0.5° resolution grid of the wave models every 6 h.

The differences between the two wind fields (reanalyzed ARPEGE and ECMWF) may come from (i) the model itself and its associated assimilation method, (ii) the number of standard observations that were assimilated (only data that arrived in time for the real-time analysis have been used for the ECMWF winds), or (iii) the assimilation of *ERS-1* scatterometer data in the case of the reanalyzed ARPEGE winds.

Table 2 shows a comparison of the reanalyzed ARPEGE wind speeds and the ECMWF wind speeds with the observations from the altimeters of the TOPEX/Poseidon and *ERS-1* satellites during October 1993. The mean differences between modeled and observed winds are a few centimeters per second and the standard deviations are of the order of 2 m s^{-1}. These results are significant at the 99% confidence level because of the large database available. The mean differences and standard deviations are of the same order of magnitude for both wind fields, which seems to show that both wind fields are of the same quality. However, the correlation between modeled and observed winds is higher for the ECMWF winds. As a consequence, we will focus here on the results obtained when driving the wave models with the ECMWF winds. It should be noted that runs were also performed by forcing VAG and WAM with the reanalyzed ARPEGE winds in order to study the impact of the winds on the results of the wave models.

4. Comparison between the results of the VAG and of the WAM

Two hindcasts were performed by forcing VAG and WAM by the ECMWF winds during October 1993 on the entire North Atlantic. In this section we compare the results of these two hindcasts.

a. General comparison of the SWHs

The analysis of the wave fields for the whole period showed that the structure of the SWH fields is quite similar in both models. Particularly, the positions and shapes of the areas of high SWHs are very close in VAG and WAM. This agreement was confirmed by a statistical comparison between VAG and WAM SWHs at all sea points every 3 h during October 1993 (3 888 144 data for each model): the correlation coefficient obtained is 0.92. However, WAM SWHs are about 13 cm lower than those for VAG (mean SWHs are, respectively, 2.41 and 2.28 m for VAG and WAM). So the variations of the SWHs in both models is similar but with a systematic mean difference between VAG and WAM.

These results are confirmed by a statistical comparison of the SWHs hindcasted by VAG and WAM (with both models forced by the ECMWF winds) with the measurements from TOPEX/Poseidon and *ERS-1*. Satellite observations and models data were collocated, as explained in section 3b. The result of this comparison is summarized in Table 3.

For the hindcasts run with the ECMWF wind fields, and those run with WAM using the version without wind–wave coupling, the mean differences between the models' SWHs and those of the satellites are small and of the same order of magnitude for both models (0.07 to 0.08 m for VAG; −0.06 to −0.11 m for WAM). However, when WAM is used in its complete cycle 4 version (with the wind–wave coupling) a significant negative bias is found with respect to the satellite data

TABLE 3. Statistics of collocated datasets of SWHs hindcasted by VAG and WAM (with or without the wind–wave coupling) both forced by the ECMWF winds (first two lines) and satellite measurements. The fourth line is relative to the modified VAG model and is discussed in section 5. Mean differences and standard deviations are in meters. The collocated datasets contain 15 632 collocated points for TOPEX/Poseidon and 12 398 points for *ERS-1*. The mean SWHs and standard deviation are, respectively, 2.40 and 1.19 m for TOPEX/Poseidon, 2.54 and 1.28 m for *ERS-1*, 2.47 and 1.22 m for VAG SWHs collocated with TOPEX/Poseidon, 2.34 and 1.12 m for WAM SWHs collocated with TOPEX/Poseidon, 2.21 and 1.10 m for WAM with the wind–wave coupling SWHs collocated with TOPEX/Poseidon, 2.16 and 1.16 m for the modified VAG SWHs collocated with TOPEX/Poseidon, 2.62 and 1.20 m for VAG SWHs collocated with *ERS-1*, 2.43 and 1.10 m for WAM SWHs collocated with *ERS-1*, 2.30 and 1.08 m for WAM with the wind–wave coupling SWHs collocated with *ERS-1*, and 2.27 and 1.13 m for the modified VAG SWHs collocated with *ERS-1*.

	TOPEX/Poseidon			*ERS-1*		
	Mean difference	Std dev	Correlation	Mean difference	Std dev	Correlation
VAG	0.07	0.56	0.892	0.08	0.63	0.873
WAM	−0.06	0.49	0.911	−0.11	0.57	0.895
WAM with wind–wave coupling	−0.19	0.48	0.916	−0.24	0.56	0.901
Modified VAG	−0.24	0.52	0.902	−0.27	0.59	0.888

(−0.19 and −0.24 m with respect to TOPEX/Poseidon and *ERS-1*, respectively). A negative bias is also found for WAM with respect to the satellite data when WAM is driven by the reanalyzed ARPEGE winds [−0.23 and −0.29 m with respect to TOPEX/Poseidon and *ERS-1*, respectively, whereas for the same wind field VAG presents only a very small bias (−0.04 m)]. So it seems that the trend of WAM is to underestimate the significant wave height, which is in agreement with the slow growing rate of new wind–sea mentioned in section 2c. In comparison, the bias of the significant wave heights of VAG with respect to the satellite data remains less than ±0.10 m whichever wind field used.

When one looks at the correlation between model and satellite SWHs, WAM always gives better results (higher correlation coefficients) than VAG. The differences in correlation coefficients are significant at the 99% confidence level due to the great number of points in the collocated datasets.

So if one considers the satellite observations as a reference, the WAM SWHs are slightly better when considering the correlation between models and satellites data, but VAG SWHs are more satisfactorily when considering the mean differences. Since bias in the significant wave height can most likely be removed by tuning some of the coefficients of the source/sink terms, we consider here that WAM is potentially better than VAG, in spite of the bias in the significant wave height. This study shows, however, that the WAM coefficients should be tuned to remove the bias in significant wave height.

b. Comparison between the VAG and WAM hindcasts and the SEMAPHORE measurements

In order to better understand the evolution of the sea state at the location of the SEMAPHORE experiment, we compared the major features of the wave spectra in VAG and WAM. This was achieved by partitioning the spectra into up to four wave trains by using the method proposed by Gerling (1991). Figure 7 shows the result of this partitioning for VAG and WAM at 35.5°N, 24.5°W during October 1993. This location (hereafter referred to as point M) was chosen because it is the central point of the SEMAPHORE area, where the largest number of observations were performed. The most important wave trains exist in both wave models and they are quite similar when comparing their energies and wavelengths. A northerly swell train with a 200–300-m wavelength can be observed on days 278–282, a northeasterly swell train with wavelengths around 170 m is observed from day 285 to day 293, and a westerly train with wavelengths between 100 and 150 m is visible from day 296 to day 300. Energetic wind–sea trains can be seen from days 281 to 284, 286 to 289, and 302 to 304. Most of the time, complex sea states can be observed with several wave trains coexisting, but VAG and WAM give coherent results. However, significant differences can be seen between the two models: there are more low-energy wave trains in VAG, and the transition between the different wave trains is less marked for VAG, whereas the partitioning pattern is smoother for WAM. These differences between the wave spectra hindcasted by VAG and WAM are probably due to the differences in the treatment of the nonlinear interactions in the two models. Actually, the parameterizations of these interactions used in VAG result in a continuous alignment of wind and wind–sea, which induces fast rotations of the wind–sea. This was already evidenced in the test run presented in section 2e. The VAG model also favors the separation of a wave train into several trains when the wind rotates. In contrast, the explicit calculation of the nonlinear interactions in WAM makes the wave trains smoother and makes their variations in time more slow.

Figure 8 presents the temporal evolution of the total SWH and of the peak frequency of the wave spectra hindcasted during October 1993 at point M by VAG

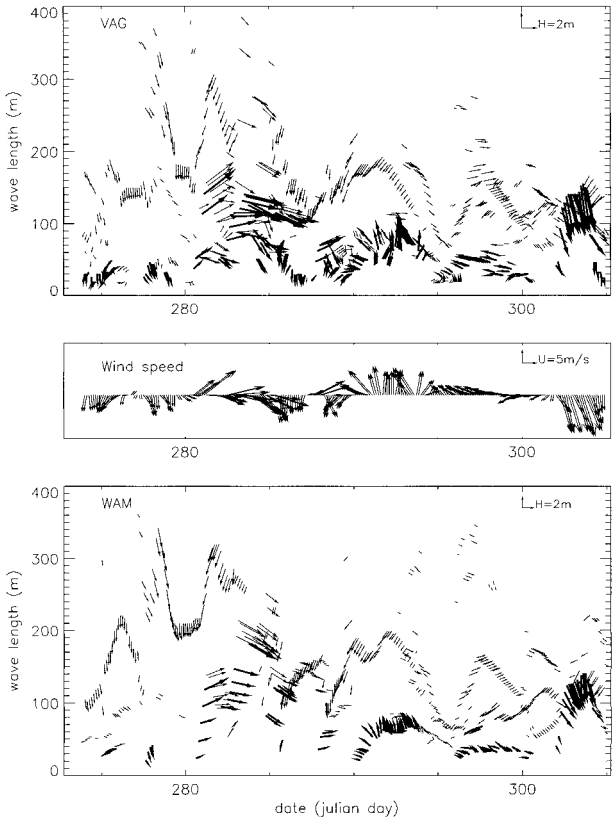

FIG. 7. Partitioning of the directional spectra obtained with VAG (top panel) and WAM (bottom panel) at point M (35.5°N, 24.5°W) during Oct 1993. Each wave train is represented by an arrow; the length of the arrow is proportional to the energy of the wave train, its direction indicates the direction to which the train propagates, and its ordinate gives the mean wavelength of the wave train. Wind–sea wave trains are plotted in bold arrows. In the middle panel, the evolution of the wind vector during Oct 1993 at point M is also shown.

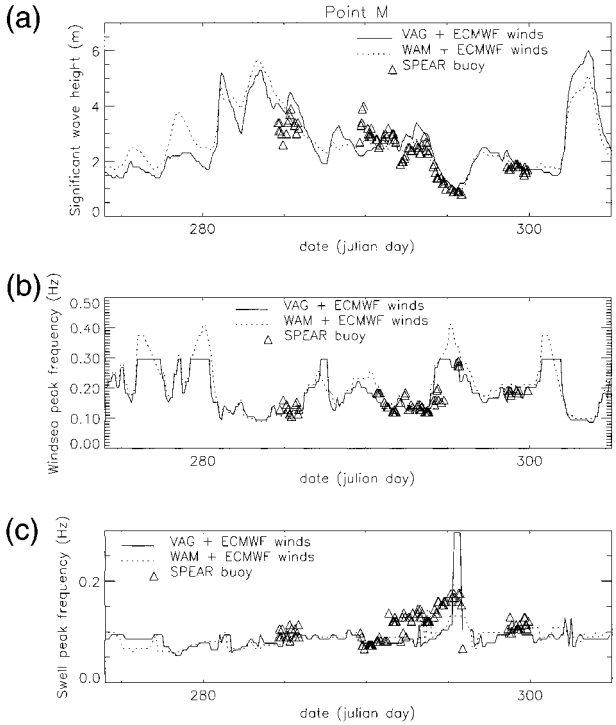

FIG. 8. Temporal evolution of (a) the SWH, (b) the wind–sea peak frequency, and (c) the swell peak frequency (bottom panel) at point M during Oct 1993. Continuous line is VAG, dotted line is WAM and triangles are the measurements made by the SPEAR buoy.

and WAM, and the corresponding measurements made by the SPEAR buoy located near point M during the SEMAPHORE experiment. Although it is difficult to achieve a quantitative comparison between buoy measurements and models hindcasts (because of the small number of data points), this figure illustrates that there is a good agreement between the hindcasted values and the buoy data, both for SWH and peak frequency. The only important disagreement is observed on 16 October, when the hindcasted SWHs are much lower than the measured ones (about 2.4 vs 4 m), regardless of the wave model considered. From a comparison of the nondirectional frequency spectra of the buoy with the spectra of the VAG and WAM models (not shown), it appears that the underestimate of the SWHs of the models at the location of the buoy is due to an underestimate of the energy of the swell component. Due to the lack of data in the generation zone of this swell (northeast of the buoy measurements), no clear explanation of this temporary disagreement could be found, which occurs for both models.

We also performed a comparison of directional spectra obtained from VAG and WAM with those derived from the observations of the airborne radar RESSAC. From these radar observations, directional spectra are retrieved for wavelengths in the range 50–400 m (frequencies from 0.06 to 0.17 Hz) with a 10% accuracy in wavelength and with a 15° resolution in direction (with, however, a 180° ambiguity in the propagation direction). The absolute level of the spectra and the associated significant wave height must be interpreted with caution because the transfer function, which is applied to convert the direct measurements (spectra of backscattered modulation) to wave spectra, is not well known. So, we restrict our comparisons here to the spectral behavior (in a relative sense). Figure 9 illustrates the results for the case of the wave spectrum measured by RESSAC on 20 October at 1525 UTC and the corresponding spectra from VAG and WAM. Although the spectra are quite complex, both models do reproduce the three different wave systems observed by RESSAC (note that the 180° ambiguity for the RESSAC spectra is not removed in the plot of Fig. 9.). This good agreement was noted for all spectra measured by RESSAC during October and November 1993 (about 30 spectra).

5. Modifications of the VAG model

Some weaknesses of the VAG model were evidenced by studying the growth and decay curves (section 2).

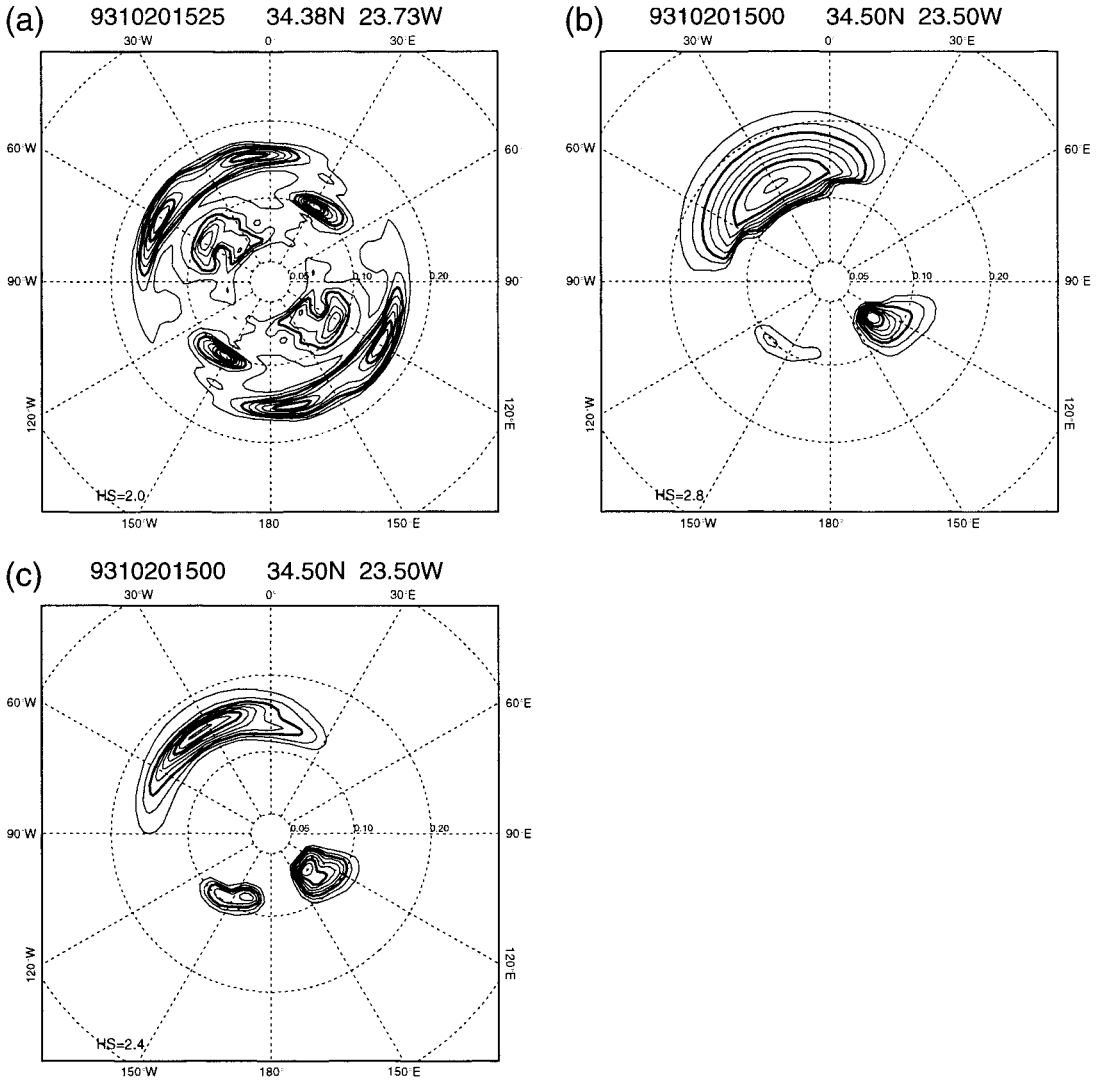

FIG. 9. (a) Directional spectrum of the waves measured with the airborne radar RESSAC on 20 Oct at 1525 UTC and corresponding spectra obtained with (b) VAG and (c) WAM. The spectra are normalized and the isolines are plotted from 0.1 to 0.9 every 0.1. The distance to the center of the plot is proportional to the frequency of the waves. The SWH is given at the bottom of each spectrum. Note that the RESSAC data are obtained with a 180° ambiguity in the propagation direction that was not removed in the figure.

Moreover, a statistical comparison of the SWHs hindcasted by VAG and WAM with the satellites measurements (section 4) showed that the WAM SWHs were better correlated with the TOPEX/Poseidon and *ERS-1* data, although they presented a significant mean difference. So we tried to remedy these weaknesses of VAG by testing some modifications.

The study of VAG and WAM growth and decay curves showed that the energy balance in the VAG model was not very satisfactory (section 2). Two main weaknesses of VAG were evidenced. First, the linear growth term was too high, whereas the exponential growth term and the dissipation term were too low compared to WAM. Second, the energy input due to the wind and the energy output due to the breaking of the waves were not well balanced. So, a limitation of the wind–sea energy was shown to be necessary, but it was quite large and resulted in losses of energy (see sections 2c–d and Figs. 1 and 3).

In order to improve the behavior of the VAG model, we tried to make VAG have a better balance between growth and decay. This was performed by replacing the exponential growth and dissipation terms used in VAG by the ones used in WAM. Because of the differences between VAG and WAM, this could not be done without readjusting VAG, which was made by taking into account weighting coefficients for the linear growth, the exponential growth, and the dissipation. These coefficients were chosen so that the growth and decay curves of the modified VAG version were in overall good

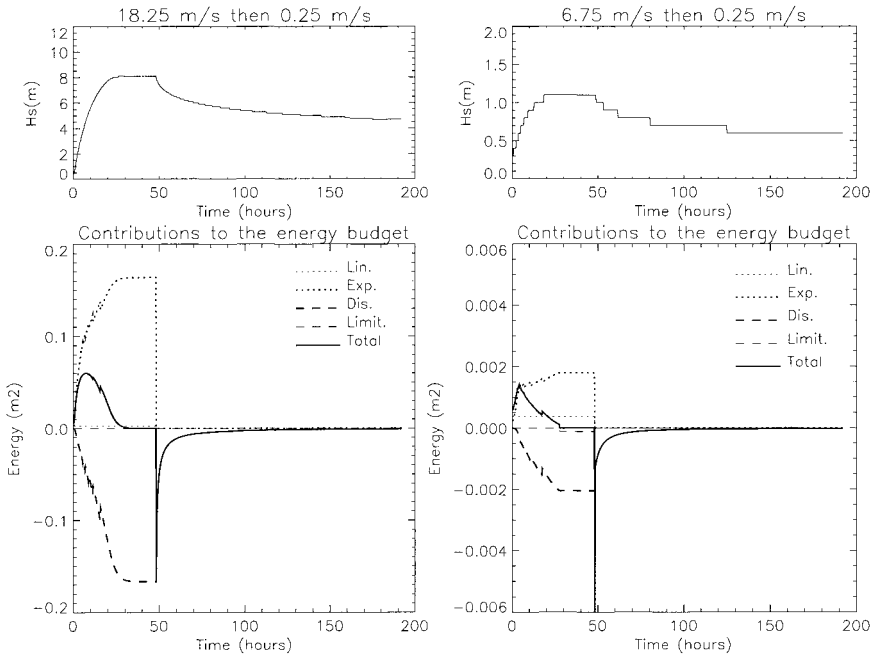

FIG. 10. As in Fig. 1, but for the modified VAG version.

agreement with VAG and WAM standard curves. This version of VAG will be referred to as the ''modified VAG'' model in the following.

The growth and decay curves obtained by driving the modified VAG model by a 18.25 m s^{-1} (6.75 m s^{-1}, respectively) wind during 48 h and then by a 0.25 m s^{-1} wind are shown in Fig. 10. These curves should be compared with those in Fig. 1, which were obtained with the VAG standard version. For the high wind speed case (18.25 m s^{-1}), the modification of VAG leads to a clear improvement of the growth and decay curves. The linear growth term is now negligible compared to the exponential growth term. This is in better agreement with experimental results (Kahma and Donelan 1988). Moreover, growth and dissipation balance better, leading to a smaller limitation of the wind–sea energy. However, the wave growth remains a little too fast (about 25 h until full development; WMO 1989). For the light wind case, the rate of the wave growth is slower for the modified VAG than for VAG and the linear growth term also remains weak, so that the energy balance is quite satisfactory. However, the limitation of the wind–sea energy remains relatively high compared to the other terms of the energy budget. In spite of this, the modification of VAG results in an overall improvement, particularly for high wind conditions.

The modification of the expressions for growth and decay in VAG had no major impact when the test described in sections 2d–f was repeated. Even with the modification of the growth and dissipation terms, the behavior of VAG is not satisfactory when changing the frequency of the wind forcing or in case of wind rotations: the losses of energy due to the limitation of the wind–sea energy remain.

So this modification of VAG has a positive impact on the behavior of VAG, but it does not solve the problem of the high sensibility of the model to the frequency of the wind driving. This shortcoming is probably not restricted to the VAG model but rather inherent to second-generation models because of the constraint that must be imposed in this case on the wind–sea part of the wave spectrum. This shows that some care must be taken for these models if changes in the forcing have to be done.

6. Hindcasts with the modified VAG model

Hindcasts were performed with the modified VAG model for October 1993 on the North Atlantic to assess the improvements resulting from the modification of VAG. In these hindcasts the weighting coefficients of the sink/source terms are those determined from the idealized case presented in section 5. They have not been precisely tuned because this would have required the use of a large dataset of real cases and this was out of the scope of the study presented here.

The first hindcast was performed by forcing the modified VAG model by the ECMWF winds every 6 h (the same hindcast was also performed using the ARPEGE reanalyzed winds). A comparison between the SWHs hindcasted by the standard and the modified VAG models showed that the impact of modifying VAG was principally a decrease of the SWHs (mean difference and correlation between both datasets are, respectively,

−0.30 m and 0.977), which is probably due to the fact that the weighting coefficients in the modified VAG have not been precisely tuned. However, the comparison between the SWHs hindcasted by both versions of VAG and the SWHs measured by TOPEX/Poseidon and *ERS-1* showed that the modification of the VAG model results in better correlation between VAG SWH and satellites SWHs (see the last line of Table 3).

The mean differences between modified VAG outputs and satellites data are important (−0.24 to −0.27 m), but this is probably because the weighting coefficients for the linear growth, the exponential growth, and dissipation in the modified VAG were not precisely adjusted. In contrast, the standard deviations decrease when modifying VAG but they remain slightly higher than those obtained with WAM. The improvement in correlation when modifying VAG (0.902 instead of 0.892 and 0.888 instead of 0.873) is significant due to the large number of data in the collocated datasets. The performances of the modified VAG model—when considering the correlation coefficients—are intermediate between those of the standard VAG and WAM models. So the modification of VAG results in a significant improvement of its performances, when correlation coefficients are considered.

We also have estimated the influence of the modification of the VAG model on its sensitivity to the frequency of the wind driving. We therefore performed a second hindcast with the modified VAG model by driving it with wind fields interpolated every 15 min. The comparison of the SWHs obtained as outputs of the two simulations with the SWHs measured by the satellites showed that the modification of the VAG model has almost no impact on its sensitivity to the wind driving frequency, confirming the conclusion of section 5.

The run tests discussed in section 5 showed that the modification of the VAG model resulted in a better balance between growth and decay, so that the limitation of the wind–sea energy was reduced, especially for high wind speeds. This improvement of the VAG model was also evidenced when looking at the losses of energy resulting from the limitation of the wind–sea energy. Figure 11 shows these cumulated losses of energy on 16 October between 0300 and 0600 UTC for the VAG and the modified VAG models. The important losses evidenced in the VAG model remain with the modified version (northeast of the SEMAPHORE area, North Sea), but the total extent of areas associated to losses of energy is significantly reduced with the modified version (see Fig. 11, bottom panel cf. top panel). This reveals a significant improvement of the modified VAG model with respect to the standard version.

7. Summary and conclusions

The behavior of the standard VAG and WAM models were studied using simple tests and a comparison of hindcasts results with the observations collected during the SEMAPHORE experiment.

The study of the growth curves obtained for both models showed that the wave growth is too fast in the standard VAG for high wind speeds, but it is too slow in WAM for low wind speeds. Moreover, the evolution of the wave spectrum in VAG is not very satisfactory when the wind rotates, particularly for instantaneous rotations of the wind and small time steps. In such cases, the partitioning of the spectrum into wind–sea and swell seems to be more realistic in WAM than in VAG. Finally, the tests evidenced a high sensitivity of VAG to the frequency of the wind forcing, which is not satisfactory. This shortcoming is probably not restricted to the VAG model but probably inherent to second-generation models because of the constraint that must be imposed in this case on the wind–sea part of the wave spectrum.

The comparison of the results of a one-month hindcast obtained with VAG and WAM with each other and with observations collected during the SEMAPHORE experiment showed that both models give overall similar results in terms of significant wave height. The wave fields and spectra hindcasted by VAG and WAM are generally consistent. Moreover, the significant wave heights and the spectral behavior (peak frequency and direction) obtained with VAG and WAM are in overall good agreement with those measured by the SPEAR buoy or the airborne radar RESSAC during the SEMAPHORE experiment. The only discrepancy between models outputs and measurements was observed on 16 October, but no clear reason could be found and both models exhibited the same problem in this situation. So, VAG and WAM give good predictions of the evolution of the sea state.

The comparison of the SWHs hindcasted by VAG and WAM with the ones measured by TOPEX/Poseidon and *ERS-1* evidenced that WAM SWHs are better correlated with the satellites ones but present a larger negative bias, in particular when the wind/wave coupling is kept in WAM (as in the operational cycle 4 version of WAM).

Some modifications of VAG were also tested. The purpose of these modifications was to tend to a better balance between growth and decay when the waves are fully developed. This could be partly achieved by using the same expressions in VAG to describe growth and decay as the ones used in WAM. Although the coefficients of the modified VAG have not been precisely tuned, there were some improvements. The balance between growth and decay is significantly better, which results in less loss of energy in the model and in a more realistic growth curve. However, VAG remains very sensitive to the frequency of the wind driving. Hindcasts made with the modified VAG result in a better correlation between satellite and VAG significant wave heights, with respect to the standard version. The bias is, however, larger than in the previous version of VAG.

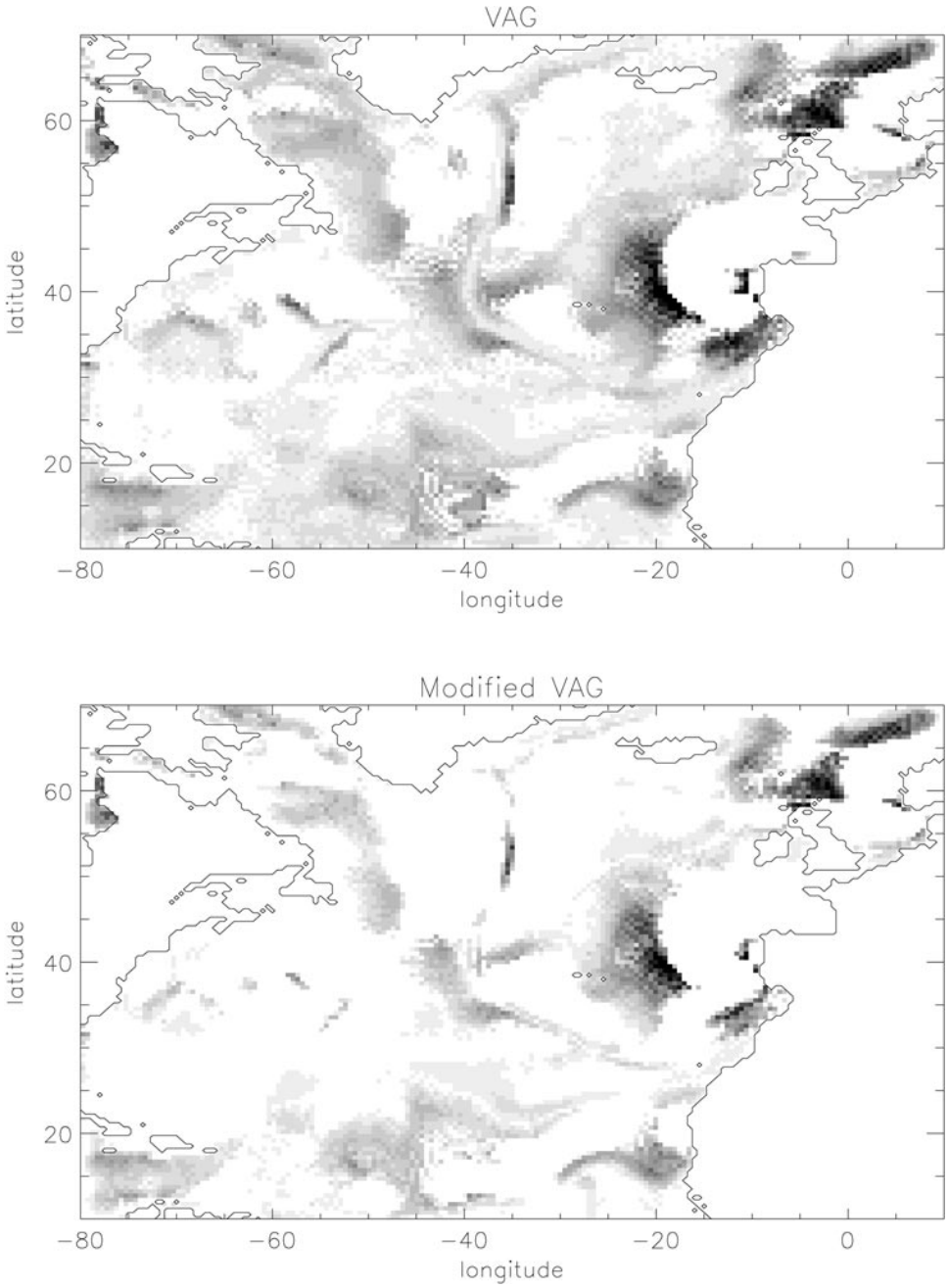

FIG. 11. Fields of the energy losses summed between 0300 and 0600 UTC on 16 Oct for (a) the standard VAG model and (b) the modified VAG model. These energies have been converted into SWHs by using $\text{SWH} = 4.004\sqrt{\text{Energy}}$. White points mean no energy losses and black points mean losses corresponding to SWHs greater than 3 m. In the other cases, gray shades are proportional to the SWHs corresponding to the energy losses.

This bias should be removed by tuning more precisely the coefficients—but this requires a study on a larger database that was out of the scope of this paper. The better correlation with satellite data suggests that the modified VAG gives better results than the standard version. The correlation with satellite data tends to be also closer to the results obtained with WAM. From this modified VAG version we conclude that the differences between the standard VAG and WAM performances were not only due to the differences in the treatment of the nonlinear interactions but to differences in the parameterizations of the source and sink terms.

We are aware, however, that these conclusions should be confirmed by adjusting the modified VAG and performing a new additional comparison between VAG and WAM using a more important dataset. This study was based principally on SWHs and it should be continued by a study of the wave spectra. This is particularly important in the case of nonstationary situations where the advantage of the third-generation WAM model could be more obvious. This is, however, difficult to achieve because of the small number of observations available for validation.

This study showed that although some shortcomings can be seen when using a second-generation model, the differences in the hindcasted wave fields obtained from of a second-generation and from a third-generation model are small. Since second-generation models like VAG are much easier to implement and use with less CPU time, this shows that the choice between second-generation and third-generation models is not obvious. The development of data assimilation into wave models for operational use makes this question still open because a trade-off will have to be found between the degree of complexity of the model and the degree of complexity of the assimilation technique. It is likely that in the future, some improvements in the sea state prediction will mainly come from an efficient assimilation technique. In this paper we showed that second-generation models are still valuable tools for wave prediction if the wind input and dissipation terms are accurate. So it may be a suitable choice to develop data assimilation schemes into second-generation models that are much more simple to handle than third-generation ones because of the treatment of the nonlinear interaction term.

Acknowledgments. The SEMAPHORE experiment was supported by several French organizations: CNRS-INSU, DRET, Météo-France, IFREMER, SHOM, and CNES. Financial support from the European Space Agency was also obtained. Part of this work was performed under the Contract DRET 93141. The authors wish to thank Jean Tournadre from IFREMER who provided the satellite data, and all the scientific and technical teams who participated in the SEMAPHORE experiment.

APPENDIX

Expressions Used in VAG and WAM for the Sink/Source

a. Definition of variables

f	Frequency
$f_{\max}$	Maximum frequency in the model
θ	Direction of propagation
θ_w	Direction of the wind
U	Wind speed
ρ_a, ρ_w	Densities of air and water, respectively
c	Phase velocity of the spectral component
E	Total energy of the spectrum
u_*	Friction velocity
τ	Wind stress
τ_w	Wave-induced stress

b. Expressions used in VAG

The source term used in VAG is the sum of four terms:

- a linear growth term given by (Golding 1983)

$$\begin{cases} S_{\text{lin}}(f, \theta) = 3.18 \times 10^{-6} \dfrac{2}{\pi} U^2 \cos^2(\theta - \theta_w) & \text{if } f = f_{\max} \text{ and } |\theta - \theta_w| < 90^\circ, \\ 0 & \text{otherwise.} \end{cases} \tag{A1}$$

- an exponential growth term given by (Snyder et al. 1981)

$$\begin{cases} S_{\text{exp}}(f, \theta) = 0.054 \left\{ 2\pi f \dfrac{\rho_a}{\rho_w} \left[\dfrac{U \cos(\theta - \theta_w)}{c} - 1 \right] F(f, \theta) \right\} & \text{if } \dfrac{U \cos(\theta - \theta_w)}{c} > 1, \\ 0 & \text{otherwise.} \end{cases} \tag{A2}$$

- a dissipation term given by (Golding 1983)

$$S_{\text{dis}}(f, \theta) = 4 \times 10^{-4} f^2 E^{0.25} F(f, \theta), \text{ and} \tag{A3}$$

- a parameterization of the nonlinear interactions in two steps: limitation of the wind–sea energy and reshaping of the wind–sea spectrum.

c. Expressions used in WAM

The source term used in WAM is the sum of three terms:

- an exponential growth term given by (Janssen 1991)

$$S_{\exp}(f,\theta) = \begin{cases} 2\pi f \dfrac{\rho_a}{\rho_w} \dfrac{1.2}{0.41^2} \mu(\ln\mu)^4 x^2 F(f,\theta) \\ \qquad \text{if } \mu < 1 \\ 0 \qquad \text{otherwise,} \end{cases} \tag{A4}$$

with

$$\mu = \frac{g z_0}{u_*^2}\left(\frac{u_*}{c}\right)^2 e^{0.41/x} \tag{A5}$$

$$x = \left(\frac{u_*}{c} + 0.011\right)\cos(\theta - \theta_w) \tag{A6}$$

$$z_0 = \frac{0.01 u_*^2}{g\sqrt{1 - \dfrac{\tau_w}{\tau}}} \tag{A7}$$

$$u_* = \frac{0.41U}{\ln\left(\dfrac{10}{z_0}\right)}. \tag{A8}$$

In the the WAM cycle 4 version, u_* is computed iteratively because τ_w depends on $S_{\exp}$.

In the runs we have made with the wind–wave coupling we used the following expressions:

$$\tau_w = 0 \qquad u_* = \sqrt{C_d}U \tag{A9}$$

with

$$C_d = \begin{cases} 1.2875 \times 10^{-3} & \text{if } U < 7.5 \text{ m s}^{-1} \\ (0.8 + 0.065U) \times 10^{-3} & \text{otherwise.} \end{cases}$$

(Wu 1982) (A10)

- a dissipation term given by (Hasselmann 1974; Komen et al. 1994)

$$S_{\text{dis}}(f,\theta) = -2.25\frac{(2\pi)^9}{g^4} f_m^9 E^2 \left[\left(\frac{f}{f_m}\right)^2 + \left(\frac{f}{f_m}\right)^4\right] F(f,\theta), \tag{A11}$$

  where f_m is the mean frequency of the spectra defined by $f_m = [(1/E)\iint f^{-1}F(f,\theta)\,df\,d\theta]^{-1}$, and
- an explicit computing of the nonlinear interactions (Hasselmann et al. 1985; Burgers 1990).

REFERENCES

Burgers, G., 1990: A guide to the Nedwam wave model. Scientific Rep. WR-90-04, KNMI, De Bilt, 81 pp. [Available from the Koninklijk Nederlands Meteorologisch Instituut, Library of the KNMI, P.O. Box 201, 3730 AE De Bilt, Netherlands.

Courtier, P., C. Freydier, J.-F. Geleyn, F. Rabier, and M. Rochas, 1991: The ARPEGE project at Météo-France. *Proc. ECMWF Seminar*, Vol. II, Reading, United Kingdom, CNRM/GMAP, 193–231.

Donelan, M. A., and W. J. Pierson, 1987: Radar scattering and equilibrium ranges in wind-generated waves with application to scatterometry. *J. Geophys. Res.*, **92** (C), 4971–5029.

——, J. Hamilton, and W. H. Hui, 1985: Directional spectra of wind generated waves. *Philos. Trans. Roy. Soc. London*, **315A,** 509–562.

Eymard, L., and Coauthors, 1996: Study of the air–sea interactions at the mesoscale: The SEMAPHORE experiment. *Ann. Geophys.*, **14,** 986–1015.

Gerling, T. W., 1991: A comparative anatomy of the LEWEX wave systems. *Directional Ocean Wave Spectra*, R. C. Beal, Ed., The John Hopkins University Press, 182–193.

Golding, B., 1983: A wave prediction system for real-time sea state forecasting. *Quart. J. Roy. Meteor. Soc.*, **109,** 393–416.

Guillaume, A., 1990: Statistical tests for the comparison of surface gravity wave spectra with application to model validation. *J. Atmos. Oceanic Technol.*, **7,** 552–567.

Günther, H., S. Hasselmann, and P. A. E. M. Janssen, 1992: *Wamodel—Cycle 4* (revised version). Deutsches Klimarechenzentrum Tech. Rep. 4, 103 pp. [Available from DKRZ, Modell Betreuungsgruppe, Bundesstrasse 55, D-20146 Hamburg, Germany.]

Hasselmann, K., 1962: On the non-linear energy transfer in a gravity-wave spectrum, Part 1: General theory. *J. Fluid Mech.*, **12,** 481–500.

——, 1974: On the spectral dissipation of ocean waves due to whitecapping. *Bound.-Layer Meteor.*, **6,** 107–127.

——, and Coauthors, 1973: Measurements of wind-wave growth and swell decay during the Joint North Sea Wave Project (JONSWAP). *Deut. Hydrogr. Z. Suppl. A,* **8** (12), 95 pp.

Hasselmann, S., and K. Hasselmann, 1984: The wave model EXACT-NL. *Ocean Wave Modeling*, The SWAMP Group, Ed., Plenum Press, 249–251.

——, K. Hasselmann, J. H. Allender, and T. P. Barnett, 1985: Computations and parameterizations of the nonlinear energy transfer in a gravity wave spectrum. Part II: Parameterizations of the nonlinear energy transfer for application in wave models. *J. Phys. Oceanogr.*, **15,** 1378–1391.

Hauser, D., and G. Caudal, 1996: Combined analysis of the radar cross-section modulation due to the long ocean waves around 14° and 34° incidence: Implication for the hydrodynamic modulation. *J. Geophys. Res.*, **101,** 25 833–25 846.

——, ——, J. Rijckenberg, D. Vidal-Madjar, G. Laurent, and P. Lancelin, 1992: RESSAC: A new airborne FM/CW radar ocean wave spectrometer. *IEEE Trans. Geosci. Remote Sens.*, **30,** 981–995.

Holt, M., 1994: An intercomparison of the WAM and UKMO wave models run at the United Kingdom MetOffice. United Kingdom MetOffice, Forecasting Research Division Tech. Rep. 120, 12 pp. [Available from The Meteorological Office, Forecasting Research Division, London Road, Bracknell, Berkshire RG12 2SZ, United Kingdom.]

Janssen, P. A. E. M., 1989: Wave-induced stress and the drag of air flow over sea waves. *J. Phys. Oceanogr.*, **19,** 745–754.

——, 1991: Quasi-linear theory of wind wave generation applied to wave forecasting. *J. Phys. Oceanogr.*, **21,** 1631–1642.

Kahma, K. K., and M. A. Donelan, 1988: A laboratory study of the minimum wind speed for wind wave generation. *J. Fluid Mech.*, **192,** 339–364.

Komen, G. J., L. Cavaleri, M. Donelan, K. Hasselmann, S. Hasselmann, and P. A. E. M. Janssen, 1994: *Dynamics and Modelling of Ocean Waves.* Cambridge University Press, 532 pp.

Le Meur, D., H. Roquet, J. M. Lefèvre, B. Fradon, and J. Tournadre, 1994: Preliminary study of the impact of *ERS-1* scatterometer wind data on numerical wave modeling. *Proc. Oceans 94 OSATES*, Brest, France, IEEE, 88–93.

Longuet-Higgins, M. S., 1969: On wave breaking and the equilibrium spectrum of wind-generated waves. *Proc. Roy. Soc. London*, **310A,** 151–159.

Miles, J. W., 1957: On the generation of surface waves by shear flows. *J. Fluid Mech.*, **3,** 185–204.

Phillips, O. M., 1957: On the generation of waves by turbulent wind. *J. Fluid Mech.*, **2,** 417–445.

——, 1977: *The Dynamics of the Upper Ocean*. 2d ed. Cambridge University Press, 336 pp.

——, 1985: Spectral and statistical properties of the equilibrium range in wind-generated gravity waves. *J. Fluid Mech.*, **156,** 506–531.

Pierson, W. J., and L. Moskowitz, 1964: A proposed spectral form for fully developed wind sea based on the similarity theory of S. A. Kitaigorodskii. *J. Geophys. Res.*, **69,** 5181–5190.

Snyder, R. L., F. W. Dobson, J. A. Elliott, and R. B. Long, 1981: Array measurements of atmospheric pressure fluctuations above surface gravity waves. *J. Fluid Mech.*, **102,** 1–59.

Tournadre, J., B. Chapron, and R. Abdellaoui, 1994: Données spatiales, partie 1: Données de vent et de vagues. *SEMAPHORE* Rep. 6, IFREMER, 80 pp. [Available from J. Tournadre, IFREMER, BP 70, 29280 Plouzané Cedex, France.]

van Vledder, G. P., and L. H. Holthuijsen, 1993: The directional response of ocean waves to turning winds. *J. Phys. Oceanogr.*, **23,** 177–192.

WAMDI Group, 1988: The WAM Model—A third-generation ocean wave prediction model. *J. Phys. Oceanogr.*, **18,** 1775–1810.

WMO 1989: Guide to wave analysis and forecasting. WMO Rep. 702, 233 pp. [Available from WMO, 7 bis avenue de la Paix, CP 2300, 1211 Geneva 2, Switzerland.]

Wu, 1982: Wind-stress coefficients over sea surface from breeze to hurricane. *J. Geophys. Res.*, **87,** 9704–9706.

Young, I. R., S. Hasselmann, and K. Hasselmann, 1987: Computations of the response of a wave spectrum to a sudden change in wind direction. *J. Phys. Oceanogr.*, **17,** 1317–1338.